

Article

Not peer-reviewed version

Diagnosing the Controls of the 2025 Talidas GLOF Using Multi-Source Satellite Observations

[Imran Khan](#)*, [Jeremy M. Johnston](#), [Jennifer M. Jacobs](#)

Posted Date: 6 March 2026

doi: 10.20944/preprints202603.0519.v1

Keywords:

glacial lake; GLOF; snowmelt; remote sensing



Preprints.org is a free multidisciplinary platform providing preprint service that is dedicated to making early versions of research outputs permanently available and citable. Preprints posted at Preprints.org appear in Web of Science, Crossref, Google Scholar, Scilit, Europe PMC.

Copyright: This open access article is published under a [Creative Commons CC BY 4.0 license](#), which permit the free download, distribution, and reuse, provided that the author and preprint are cited in any reuse.

Disclaimer/Publisher's Note: The statements, opinions, and data contained in all publications are solely those of the individual author(s) and contributor(s) and not of MDPI and/or the editor(s). MDPI and/or the editor(s) disclaim responsibility for any injury to people or property resulting from any ideas, methods, instructions, or products referred to in the content.

Article

Diagnosing the Controls of the 2025 Talidas GLOF Using Multi-Source Satellite Observations

Imran Khan ^{1,2,*}, Jeremy M. Johnston ^{1,2} and Jennifer M. Jacobs ^{1,2}

¹ Department of Civil and Environmental Engineering, University of New Hampshire, Durham, NH 03824, United States

² Earth Systems Research Center, Institute for the Study of Earth, Oceans, and Space, University of New Hampshire, Durham, NH 03824, United States

* Correspondence: imran.khan@unh.edu

Highlights

What are the main findings?

- The 2025 Talidas GLOF followed a period of rapid lake expansion during the warmest melt season, coinciding with early and persistent snow depletion relative to the 2000-2024 baseline record.
- Multi-decadal satellite records (1992-2024) show that lakes of comparable size in earlier years did not fail abruptly, indicating that lake extent alone did not control the outburst.

What are the implications of the main findings?

- Sustained climatic anomalies and cryospheric preconditioning can destabilize moraine-dammed lakes even in the absence of a discrete trigger such as landslides.
- Multi-sensor remote sensing time series provides a robust framework for monitoring glacial lake evolution and detecting anomalous pre-GLOF conditions.

Abstract

Glacial lake outburst floods (GLOFs) are high-impact hazards in mountain regions, yet many events remain poorly documented because field access is limited and lake evolution can occur on sub-weekly time scales. Here we used high spatiotemporal resolution PlanetScope imagery (3 m) to quantify the seasonal evolution and abrupt drainage of a moraine-dammed glacial lake in August 2025 in northern Pakistan. Historical lake dynamics were reconstructed using PlanetScope (2016-2024) imagery and multi-decadal Landsat observations (1992-2018). Climatic conditions were evaluated using ERA5-Land temperature data, and seasonal snow dynamics were characterized using MODIS and PlanetScope-based snow cover analyses. Multi-decadal satellite imagery indicates that lake formation in this catchment was historically intermittent, with no evidence of abrupt drainage before 2025, highlighting the anomalous nature of the event. PlanetScope observations show steady lake expansion throughout summer 2025, reaching a maximum area of 0.052 km² prior to the GLOF on August 22. Pre- and post-event imagery reveals no discernible landslide or impact trigger. Instead, the observations are most consistent with a failure mechanism driven by meltwater-driven lake growth and overtopping or erosion of the moraine dam. The 2025 summer season (June to September) was characterized by exceptionally warm conditions and unprecedented early snow depletion relative to the 2000-2024 baseline, suggesting a strong climatic and cryospheric contribution to the outburst. These results demonstrate the value of integrating dense time series of satellite observations and climatic data for capturing glacial-lake life cycles and diagnosing likely controls on outburst initiation. The study highlights the critical role of high-frequency satellite remote sensing for improving GLOF monitoring and early-warning capabilities in data-scarce mountain environments.

Keywords: glacial lake; GLOF; snowmelt; remote sensing

1. Introduction

Glacial lakes are dynamic and potentially hazardous features in high-mountain environments, particularly under ongoing climatic warming [1–3]. Rising temperatures have accelerated glacier thinning and retreat worldwide, promoting the formation and expansion of glacial lakes [3–6]. Some glacial lakes experience sudden drainage events known as glacial lake outburst floods (GLOFs), which can generate severe downstream impacts, including channel erosion, debris deposition, infrastructure damage, and loss of life [5,7,8]. Understanding the short-term evolution of glacial lakes and the conditions leading to abrupt drainage remains a critical challenge for hazard assessment in remote mountain regions [9].

GLOFs can be initiated by a wide range of physical triggers. Short-duration or acute triggers include avalanches and landslides entering a lake, glacier calving, intense rainfall events, and rapid snowmelt leading to increased water levels and overtopping or eroding natural dams [10–14]. In contrast, longer-term processes such as progressive dam weakening, melting of buried ice within moraine dams, permafrost degradation, and internal piping can gradually destabilize lake dams, leading to failure [10,15–17]. Identifying which of these mechanisms operated during a specific event is often challenging in remote mountain settings, particularly when field observations are unavailable.

Beyond promoting lake formation and expansion, ongoing climate warming is expected to amplify GLOF triggering processes and increase the risk of GLOFs [18–20]. Warming temperatures increase meltwater input and reduce slope stability through permafrost degradation, glacier and ice-core melt, and increased debris availability, thereby enhancing the likelihood of rockfalls, landslides, debris flows, and ice avalanches entering glacial lakes and triggering GLOFs [12,20–24]. These processes can give rise to cascading hazard sequences, in which an initial mass movement generates lake overtopping or dam erosion, followed by rapid downstream flooding, channel erosion, debris deposition, and secondary damming [22,25–29]. Despite growing recognition of these compound hazards, many GLOF events in remote mountain regions remain poorly documented due to inadequate field observations [30–33].

Remote sensing has become an essential tool for monitoring glacial lakes in remote, high-altitude terrain, where field observations are sparse or often unavailable. Recent advances in satellite remote sensing and geographic information systems (GIS) now enable consistent mapping of lake formation and evolution, detection of geomorphic signatures of triggering processes, and assessment of cascading downstream impacts across local to global scales [8,14,33–35]. Such remote-sensing-based analyses combined with climatic data improve understanding of GLOF drivers and consequences and provide an essential foundation for hazard assessment, early-warning efforts, and risk mitigation in data-scarce mountain regions [22,36,37].

In this study, we use high spatiotemporal resolution PlanetScope imagery to document the evolution of a moraine-dammed glacial lake in the Talidas catchment in the Hindu Kush, Pakistan, culminating in a sudden drainage event on August 22, 2025. The GLOF triggered intense erosion along the channel, mobilizing large volumes of sediment and generating a debris flow that caused widespread destruction downstream. The massive debris deposit subsequently blocked the Gilgit River, completely obstructing its flow, leading to the formation of a large debris-dammed lake. The cascading disaster damaged more than 300 houses, agricultural land, and critical infrastructure downstream; however, an early warning from nearby shepherds prompted timely evacuation, and no fatalities were reported [38]. We analyze the seasonal development and abrupt collapse of the moraine-dammed glacial lake, geomorphic signatures of potential triggers and dam breach, and seasonal snow-covered area (SCA) dynamics to assess their relationship with lake growth. To place the 2025 GLOF in a broader context, we evaluate the historical seasonal evolution of the lake extent from the early 1990s through 2024 using a combination of Landsat (1992–2018) and PlanetScope (2016–2024) imagery, identifying years characterized by ephemeral ponding, gradual seasonal growth, or absence of lake formation. While cloud-free imagery is sparse in the earlier record, the available observations provide valuable context for evaluating the anomalous nature of the 2025 event.

This study aims to (1) quantify the seasonal evolution and abrupt drainage of the glacial lake during the 2025 melt season and analyze its historical behavior (1990s - 2024), (2) assess changes in SCA and temperature dynamics within the contributing catchment and their temporal correspondence with lake expansion, and (3) explore potential GLOF triggers (e.g., external mass movement, extreme weather events, and overtopping or erosion of the dam). Using the Talidas GLOF as a case study, which combines event-scale analysis with multi-decadal satellite observations, we demonstrate the value of high-frequency remote sensing for detecting anomalous glacial lake behavior and strengthening observational frameworks for GLOF hazard assessment in data-scarce mountain regions.

2. Materials and Methods

2.1. Study Area

This study focuses on the high-elevation moraine-dammed glacial lake that triggered the Talidas GLOF and its contributing catchment in Gilgit sub-basin of the Upper Indus Basin in northern Pakistan (Figure 1). The lake catchment, with an area of 0.8 km², is characterized by complex alpine topography and strong seasonal snow dynamics. Elevations across the catchment range from 4,700 to 5,100 m a.s.l., with steep relief and pronounced headwalls surrounding the lake basin. As per the Randolph Glacier Inventory [39], the catchment hosted a small glacier, which has now disappeared. The lake occupied a topographic depression dammed by unconsolidated moraine and debris material. This lake was located at the head of a cascading lake system, with three more lakes downstream along the main flow path (Figure S1). When the source lake drained on August 22, 2025, the downstream lakes overflowed due to the flood wave but remained structurally intact and did not undergo catastrophic drainage.

The Gilgit sub-basin forms part of the eastern Hindu Kush Range and drains into the Indus River [40]. Climatically, the region falls within a cold desert regime characterized by arid to semi-arid conditions [41]. Precipitation in the Gilgit River basin is influenced by two distinct atmospheric systems, including summer precipitation associated with the South Asian monsoon and winter-spring precipitation driven by mid-latitude westerly disturbances [42–44]. The majority of annual precipitation occurs during the winter and spring, primarily in the form of snowfall [41,42].

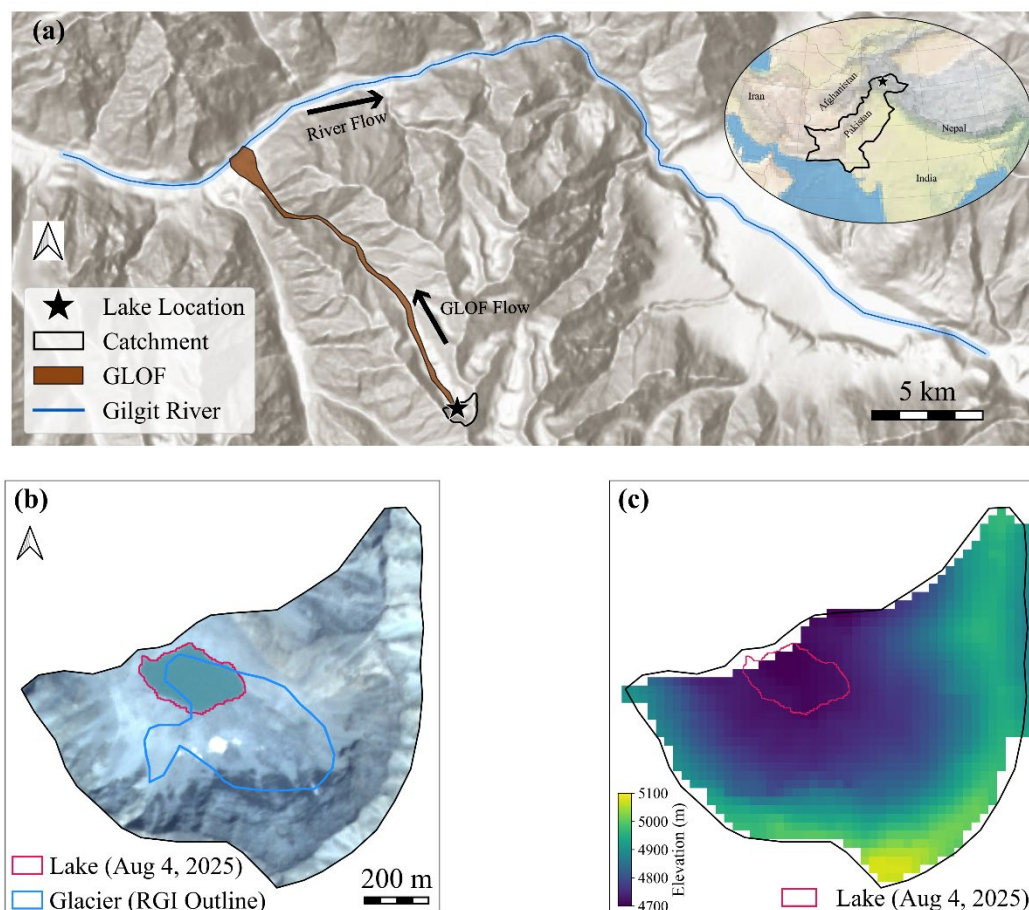


Figure 1. Overview of the study site. (a) Lake location, along with the catchment, GLOF flow path, and Gilgit River are shown on a Hillshade basemap. (b) PlanetScope true-color composite clipped to the lake catchment extent, with the pre-GLOF lake outline (August 4, 2025). The blue outline shows the Randolph Glacier Inventory glacier outline. (c) SRTM-derived elevation map for the catchment with the same lake outline overlaid.

2.2. Data

We used high-resolution PlanetScope multispectral imagery to map the glacial lake extent and SCA within the lake catchment from 2022-2025. PlanetScope imagery includes three visible bands (red, green, and blue) and one near-infrared (NIR) band at 3 m spatial resolution [45,46]. Level 3B Ortho Scene Analytic images, which are radiometrically calibrated, orthorectified, and provided at top-of-atmosphere reflectance [47,48], were obtained from the Planet Explorer platform (<https://www.planet.com/explorer/>) under Planet's Program for Education and Research (E&R) license. Cloud cover complicates accurate glacial lake delineation and snow mapping by obscuring surface features and exhibiting reflectance characteristics similar to snow in the visible and NIR bands, hampering reliable spectral discrimination [49]. To minimize this ambiguity, scenes were selected through careful visual inspection to ensure full coverage of the study area and the absence of cloud contamination.

Historical glacial lake dynamics from 1992 to 2018 were assessed using cloud-free multispectral optical satellite imagery from the Landsat missions, obtained through Google Earth Engine and courtesy of the United States Geological Survey (USGS). Specifically, Landsat 5 Thematic Mapper (TM), Landsat 7 Enhanced Thematic Mapper Plus (ETM+), and Landsat 8 and 9 Operational Land Imager (OLI) imagery at 30 m spatial resolution were used to characterize multi-decadal variations in lake presence, extent, and drainage behavior prior to the 2025 GLOF. For all Landsat sensors, Collection 2 Tier 1 calibrated top-of-atmosphere reflectance products were employed, ensuring consistent radiometric calibration and geometric accuracy suitable for long-term temporal analysis.

Summer season (June to September) snow persistence within the catchment was derived from the Moderate Resolution Imaging Spectroradiometer (MODIS) Terra Global Snow Cover product (0.01° spatial resolution) [50]. Shuttle Radar Topography Mission (SRTM) digital elevation data (30 m spatial resolution) were used to derive elevation and slope metrics for the lake catchment [51]. Daily mean 2 m air temperature (2000-2025) and daily total precipitation (August 2025) from the ERA5-Land reanalysis dataset (0.1° spatial resolution) were retrieved via Google Earth Engine and used to assess temperature variability and precipitation over the study area [52]. Daily aggregated precipitation for August 2025 was also obtained from NASA's Integrated Multi-satellitE Retrievals (IMERG) for Global Precipitation Measurement (GPM) product (0.1° spatial resolution) [53]. We also used the High Mountain Asia permafrost probability dataset (1 km spatial resolution) [54] to assess permafrost conditions within the lake catchment. A summary of all datasets, including their temporal coverage, spatial resolution, and usage in this study, is provided in Table S1.

2.3. Lake Delineation and Geomorphological Analysis

Glacial lake outlines were delineated through manual digitization using cloud-free PlanetScope and Landsat imagery in QGIS. Lake boundaries were mapped by visual interpretation of true- and false-color composites to ensure reliable identification of the lake outline in complex alpine terrain, particularly during periods of partial snow cover. For earlier years with sparse imagery, mapped lake extents represent discrete observations rather than continuous seasonal evolution.

To evaluate surface changes associated with the 2025 GLOF, cloud-free PlanetScope imagery acquired before and after the August 22 event (8 August 2025 and 22 August 2025, respectively) was compared using true- and false-color composites. The comparison focused on identifying geomorphic indicators of potential triggering processes, including changes in lake margins, textural changes on adjacent slopes, and disturbed material downstream of the lake. False-color composites incorporating the NIR band were generated to enhance contrasts between water, debris, and freshly exposed surfaces, which may indicate erosion or disturbance associated with rapid lake drainage.

2.4. SCA Mapping

For recent years (2022-2025), SCA was mapped from PlanetScope imagery using a Random Forest (RF) classifier, similar to the method detailed in Yang et al. (2023) [49], implemented in Python. RF classifiers have been widely shown to perform well for snow cover mapping from optical imagery [55–57]. Classification was performed using spectral features derived from the blue, green, red, and near-infrared (NIR) bands. Training data were generated from manually digitized polygons representing three surface classes: (1) snow, (2) exposed rock and debris, and (3) open water. To ensure robust performance across varying surface and illumination conditions, training samples were selected from multiple PlanetScope scenes spanning both early-season (high snow cover) and late-season (patchy or minimal snow) conditions. The trained model was applied consistently across all PlanetScope scenes to generate snow classifications. Binary snow masks were derived by isolating pixels classified as snow, which were subsequently used to compute SCA and fractional SCA (fSCA) within the catchment. To evaluate the performance of the RF classifier, validation was conducted using images from June 20, July 2, and July 21, 2025, which were not used in model training. Manually digitized validation polygons representing the same three land-cover classes were used to generate an independent set of labeled pixels. Classification accuracy was assessed using standard metrics including precision, recall, F1-score, and overall accuracy (Table S2).

Long-term (2000-2025) snow dynamics were assessed using MODIS data. Because the study catchment is small and fully contained within a single MODIS pixel, snow conditions were characterized using a binary approach indicating snow presence or snow-free conditions. The daily time series was then aggregated to compute the total number of snow-free days for each summer season (June to September).

2.5. Melt-Season Temperature Analysis

Daily mean 2 m air temperature data obtained from the ERA5-Land reanalysis were spatially averaged over the lake catchment for the period 2000-2025. Analyses focused on the summer season (June-September). A baseline climatology was constructed using the 2000-2024 period by computing the mean and standard deviation (SD) of daily temperatures for each calendar day. The daily temperature time series was smoothed using a 7-day centered moving average prior to analysis and 2025 temperature deviations from the baseline daily mean for the corresponding calendar day were then calculated. Exceedance statistics were derived relative to the smoothed baseline mean and standard deviation.

3. Results

3.1. Glacial Lake Evolution During the 2025 Melt Season

PlanetScope imagery shows that the lake catchment remained snow covered until mid-June 2025, with the first clear expression of the lake observed on June 19, 2025. Over the following days, the lake expanded steadily, nearly doubling and reaching an area of 0.020 km² by June 24 (Figure 2). From late June to early July, the lake exhibited a period of accelerated expansion, with the lake area increasing to 0.031 km² on July 3 and 0.035 km² on July 9. This phase corresponds to the most rapid areal growth observed during the season.

After mid-July, the rate of lake expansion gradually slowed, although the lake continued to grow. Lake area increased from 0.040 km² on July 21 to a seasonal maximum extent of 0.052 km² on August 20, indicating a transition from rapid growth to a more gradual expansion phase. Overall, the lake size expanded by more than a factor of 4 between June 19 and August 20. This growth was followed by an abrupt drainage on August 22. The imagery from August 22 shows only a small residual pond within the lake basin, after the observed GLOF.

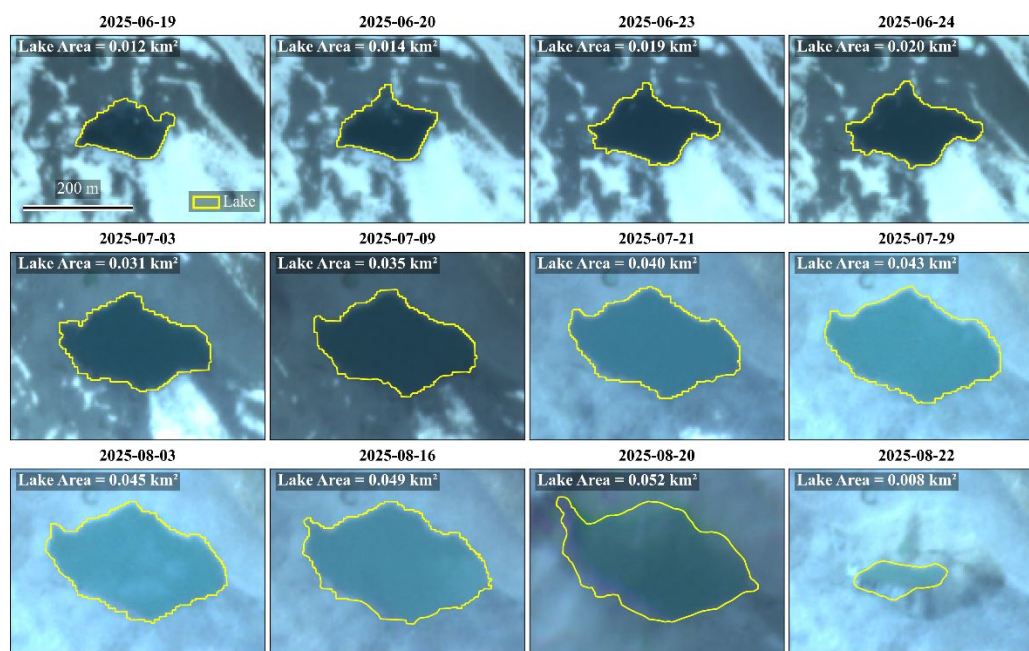


Figure 2. Evolution of the moraine-dammed glacial lake during the 2025 melt season derived from PlanetScope imagery. The lake first appears as a small surface pond on 19 June and expands progressively through July and early August. By August 22, 2025, the lake area is drastically reduced, leaving only a small residual pond.

3.2. Interannual Variability in Glacial Lake Formation and Drainage (1992-2024)

The combined Landsat (1992-2018) and PlanetScope (2016-2024) record indicates that glacial lake formation in the Talidas catchment was historically rare and highly intermittent (Figure 3). Between

1992 and 2021, most cloud-free satellite observations show no detectable lake, with only occasional small and short-lived water bodies. When present, the lake generally exhibited gradual seasonal expansion followed by progressive shrinkage rather than abrupt drainage. However, the temporal density of observations during the earlier years is sparse, particularly prior to 2016, due to the coarse revisit frequency (16-days) of Landsat satellites. Consequently, some short-lived lake occurrences may have gone undetected.

Landsat observations from 1992-2017 show only two instances of significant lake formation including a lake surface of approximately 0.037 km² on July 8, 1994, and a similar-sized lake of 0.036 km² on July 11, 2004. In 1994, useful imagery is not available to assess the seasonal lake dynamics, while in 2004, a cloud-free image in September shows no lake presence. Outside of these isolated events, the majority of cloud-free images prior to 2017 indicate either no lake or only very small ponding.

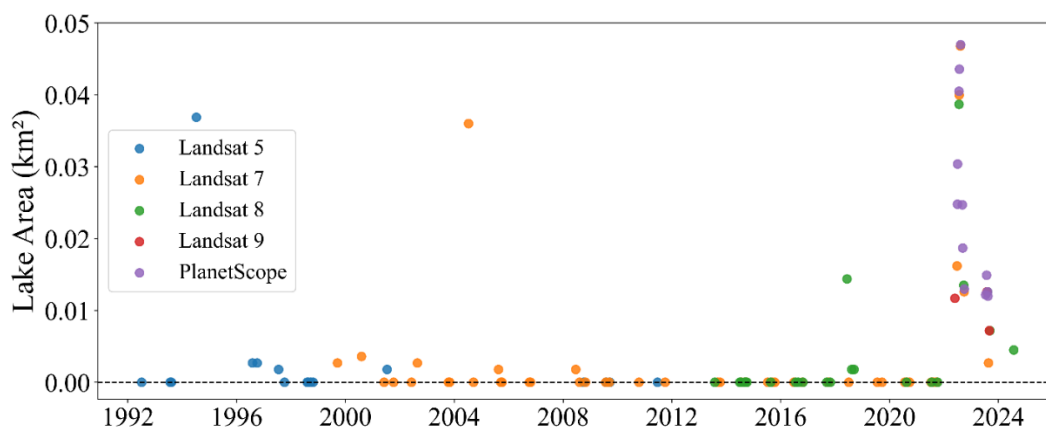


Figure 3. Multi-satellite time series of glacial lake presence and area from the early 1990s to 2024. Each point represents a single cloud-free satellite observation, with colors indicating the source sensor (Landsat 5, 7-9, and PlanetScope). Zero-area points correspond to dates when no lake was detected in a single Landsat pixel. Cloud-free imagery prior to 2018 was relatively scarce due to the coarse temporal resolution (16 days) of Landsat satellites, resulting in a lower temporal density of observations.

Higher-temporal-resolution PlanetScope imagery from 2016 onward provides a more detailed record of intra- and interannual variability in lake behavior. Between 2017 and 2021, lake formation remained infrequent, with only small and ephemeral ponds detected in most years and no observable lake in the available imagery for 2016. A clear shift occurred beginning in 2022, when a more persistent and larger lake began to develop (Figures 3, 4). In 2022, the lake was first observed in mid-June, expanded steadily through July, and reached a maximum area of approximately 0.047 km² in mid-August before gradually contracting throughout September (0.013 km² by September 30th). In 2023, the lake emerged later in the season as the seasonal snow receded, with a similar size (≤ 0.015 km²) and shape as September 2022, and contracted gradually to 0.007 km² by early September 2023. The 2024 season again showed only minor and short-lived ponding, with a maximum observed area of about 0.005 km² in July. The lake disappeared by the end of August 2024. The 2022-2024 lake life cycle shows that it developed and contracted gradually over the three-year period and disappeared in August 2024.

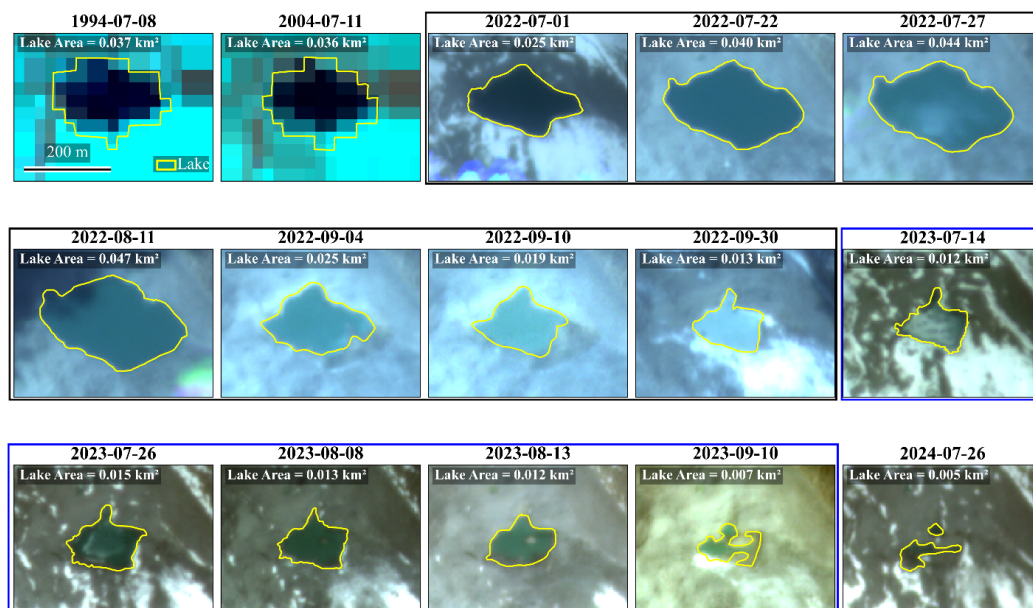


Figure 4. Landsat (1994 and 2004) and PlanetScope (2022–2024) imagery showing mapped glacial lake outlines for selected dates between 1994 and 2024. The 2022 imagery series is grouped together in the black box, while the 2023 series is in the blue box, illustrating interannual variability in lake evolution.

3.3. Climatological Context (2000–2025)

Long-term remote sensing and climatic records suggest that the lake catchment exhibits a strongly seasonal melt regime characterized by progressive warming, declining snow cover, and generally low summer precipitation. Comparison of 2025 conditions with the 2000–2024 climatology reveals that the year of the outburst represents a distinct climatic departure from the long-term climatology, with sustained anomalous warming and exceptionally early snow depletion. The climatology shows that the melt season is characterized by gradual warming from early June, peak temperatures in late July, followed by a gradual cooling period into late September (Figure 5a). There is generally low daily rainfall amounts that are fairly consistent across years during June and July with more variability for the remainder of the period (Figure 5b). Compared to the long-term climatology, daily mean air temperatures in 2025 were substantially warmer, with the seasonal mean increasing from 8.2 °C during 2000–2024 to 11.8 °C in 2025, representing a +3.6 °C deviation (Figure 5c). This value lies 3.4 standard deviations above the historical distribution and ranks as the warmest melt season in the 2000–2025 record. Daily exceedance statistics further show that 2025 was persistently warmer than normal during the melt season, except for a brief near-normal period from late July to early August. Relative to the daily climatology (mean $\pm 1SD$), 86 of 122 days in 2025 exceeded the mean + 1SD envelope and 27 days exceeded mean + 2SD, while none fell below mean – 1SD. In contrast, 2025’s cumulative precipitation was well below the climatological precipitation from June to early July. Mid-July 2025 had considerable precipitation which returned the cumulative precipitation within the climatological envelope. The remainder of the period prior to the GLOF was relatively dry except for a large multi-day rainfall event in mid-August approximately a week before the GLOF.

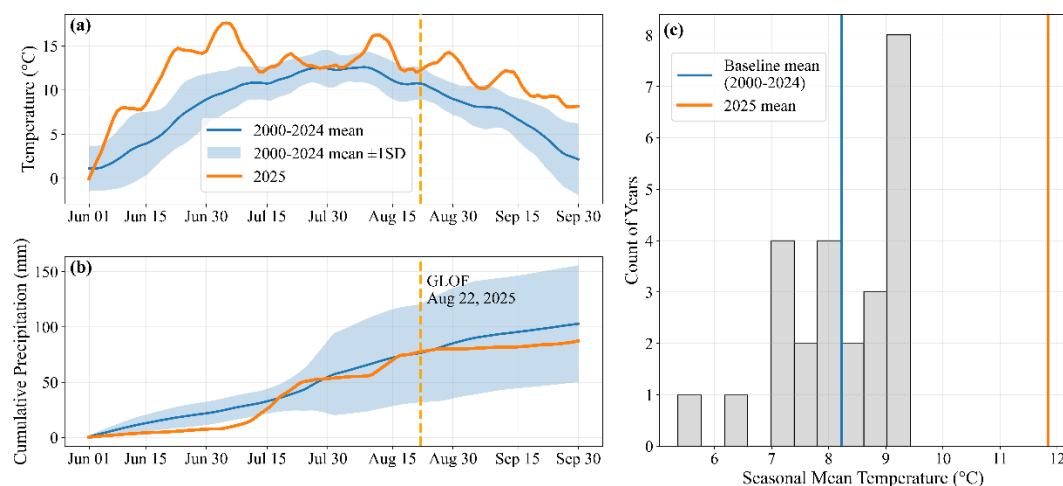


Figure 5. Climatology of the lake catchment derived from ERA5-Land temperature and GPM IMERG precipitation data. (a) Daily mean 2 m air temperature for June-September 2025 compared with the 2000-2024 climatological mean and $\pm 1SD$ envelope. The vertical dashed line marks the GLOF date (22 August 2025). (b) Cumulative precipitation for 2025 compared to the 2000-2024 climatological range. (c) Distribution of June-September mean temperatures for the 2000-2024 baseline period, with vertical lines denoting the baseline mean and the 2025 seasonal mean.

MODIS observations show that the lake catchment typically experiences a gradual transition from snow-covered to intermittently snow-free conditions during the melt season. In most years, consecutive snow-free days are concentrated between late July through early September, while snow cover persists through June and often reappears episodically during the melt season (Figure 6). For the 2000-2024 snow cover climatology, the catchment experienced an average of ~60 snow-free days, with historical values ranging from a minimum of 33 days to a maximum of 92 days. In contrast, 2025 exhibited a markedly different seasonal snow regime. The catchment transitioned to persistently snow-free conditions by early July and remained snow-free through September, resulting in 101 snow-free days, which is the highest value in the 26-year record (Figures 6, S2).

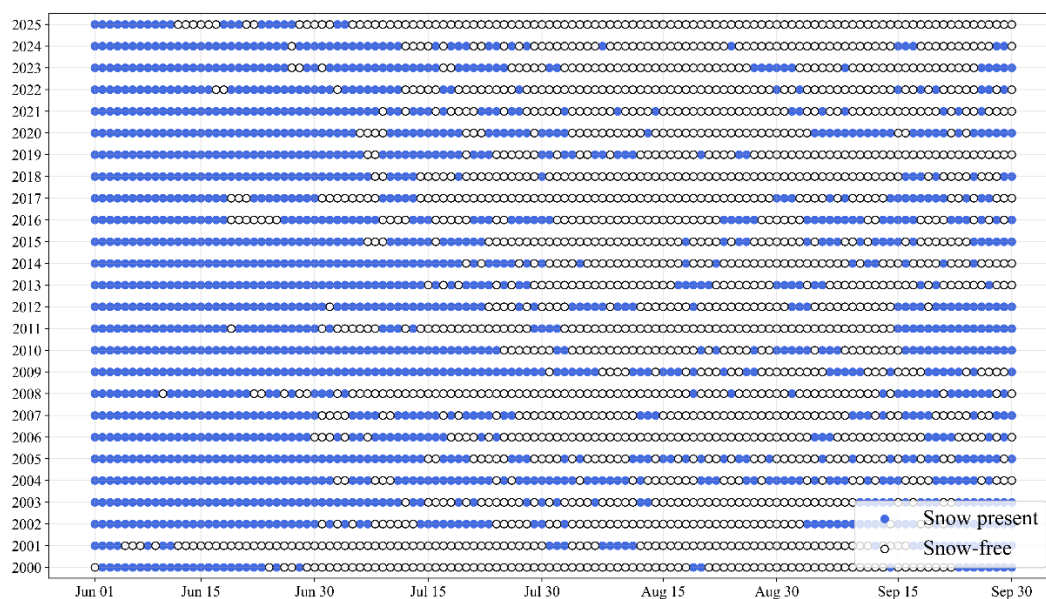


Figure 6. Daily snow presence and absence in the lake catchment from June to September for 2000-2025 derived from MODIS observations. Each point represents a single day, where blue markers indicate snow presence and

gray markers indicate snow-free conditions. The plot shows that 2025 experienced an unusually early transition to persistent snow-free conditions compared to the historical record.

3.4. Snow Dynamics and Lake Evolution (2022-2025)

High-resolution PlanetScope imagery provides detailed insight into intra-seasonal snow dynamics and lake evolution, revealing an earlier onset and a longer duration of snow-free conditions during the GLOF year as compared to other recent years (Figures 7 and S3). Across all four years from 2022 to 2025, SCA followed a generally similar seasonal trajectory, with progressive depletion from late June through late September. However, the timing and magnitude of snow loss differed among years. In 2025, fSCA decreased from moderate snow coverage (~52%) in late June to near-zero values by mid-July and remained effectively snow-free for the rest of the melt season. In contrast, during 2022, 2023, and 2024, despite rapid early-season snow loss, measurable snow cover persisted into mid-August or later. SCA at comparable stages of the melt season was lower in 2025 than in 2022, 2023, and 2024.

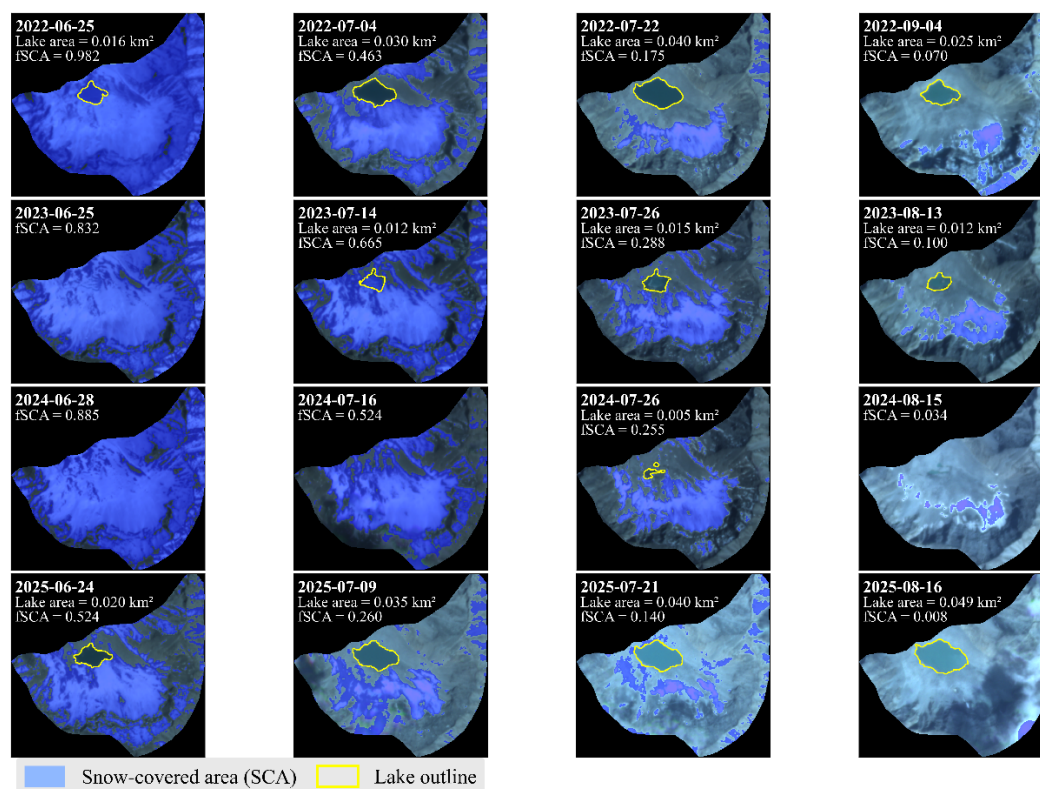


Figure 7. Seasonal evolution of SCA and the glacial lake across the 2022-2025 melt seasons, showing representative dates from late June, early July, late July, and late summer for each year. Images show progressive seasonal snow depletion and associated lake development in the catchment.

2022 and 2025 had different snow conditions and lake evolution patterns (Figure 8). In both years, initial lake expansion coincided with declining fSCA during early summer, suggesting that seasonal snowmelt was an important source of inflow. However, the subsequent trajectories diverged. In 2022, the lake reached its maximum extent around mid-August and then gradually contracted through late summer despite consistent snowmelt (Figure 8a). In 2025, rapid and near-complete snow depletion was accompanied by rapid lake expansion through June and July. The lake reached a similar maximum extent as in 2022 on a comparable seasonal timeline but instead culminated in abrupt drainage on August 22, 2025 (Figure 8b). The daily temperature comparison shows higher temperatures in 2025 compared to 2022 (Figure 8c).

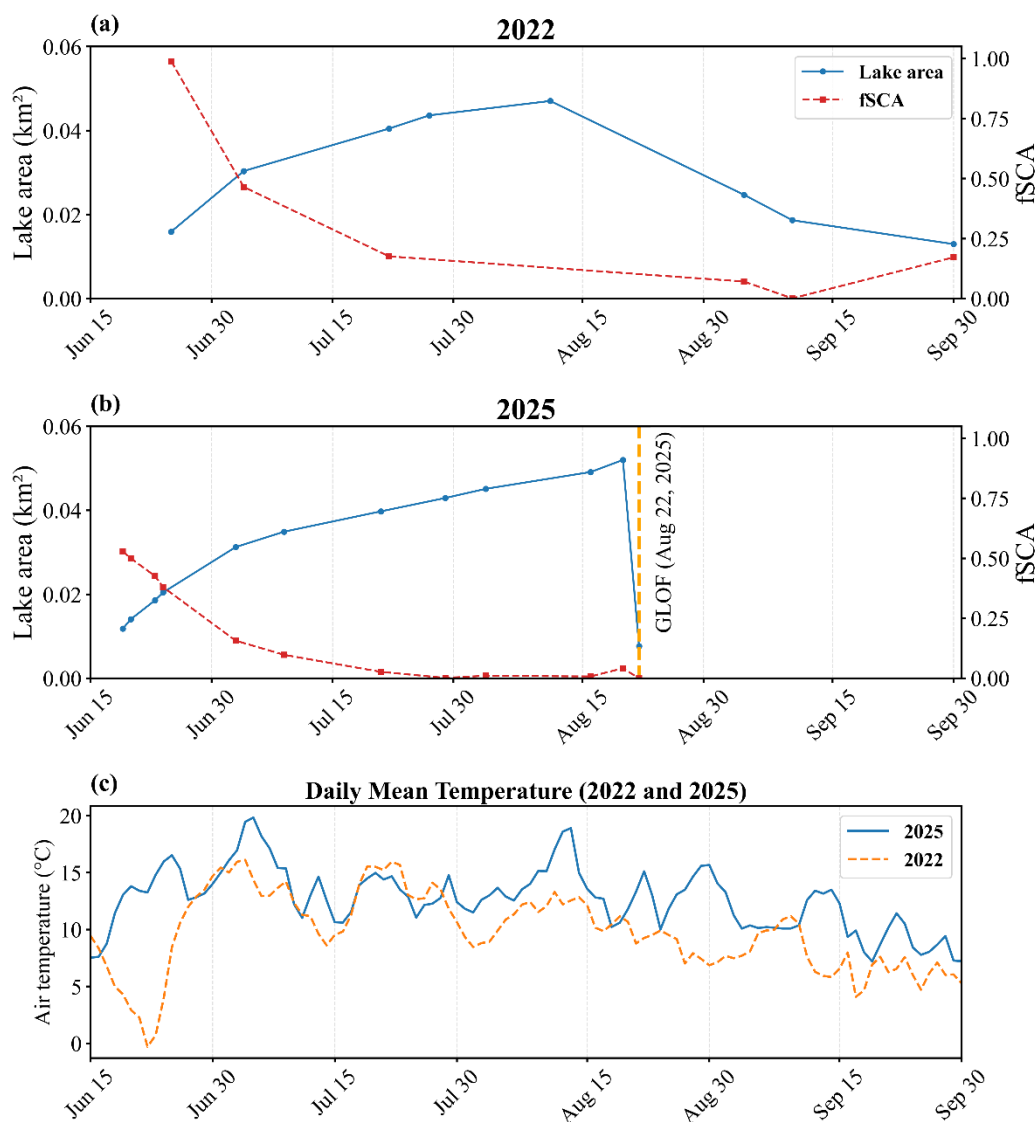


Figure 8. Seasonal evolution of lake area, fractional snow-covered area (fSCA), and air temperature for 2022 and 2025. (a) lake area and fSCA time series for 2022, characterized by gradual lake growth and seasonal contraction without abrupt drainage. (b) Time series of lake area and fSCA during the 2025 melt season, showing progressive lake expansion followed by abrupt drainage on 22 August 2025 (vertical line). (c) Comparison of daily air temperature for the summer season, showing higher temperatures in 2025 compared to 2022.

3.5. Potential GLOF Trigger

Topographic analysis based on the SRTM DEM indicates that the lake catchment is characterized by steep and highly variable terrain, with a mean slope of approximately 30° and local slopes reaching up to 68° (Figure 9a). Steep slopes surround the lake, forming near-vertical headwalls in several locations above the lake basin (Figure 9b). The High Mountain Asia permafrost dataset indicates a high probability (0.99) of near-surface permafrost occurrence within the lake catchment. Such conditions are conducive to slope instability and mass movements, particularly during warm periods where sub-surface ice may begin to thaw. However, comparison of pre- and post-event PlanetScope true- and false-color imagery reveals no clear evidence of a large landslide or coherent debris deposit on the slopes surrounding the lake (Figure 10a,b). No distinct scar or accumulation feature is detectable at PlanetScope resolution, suggesting that a major slope failure was unlikely to have directly initiated the outburst. While small, localized mass movements below the detection threshold of the imagery cannot be entirely excluded, there is no optical evidence to support a landslide-dominated trigger.

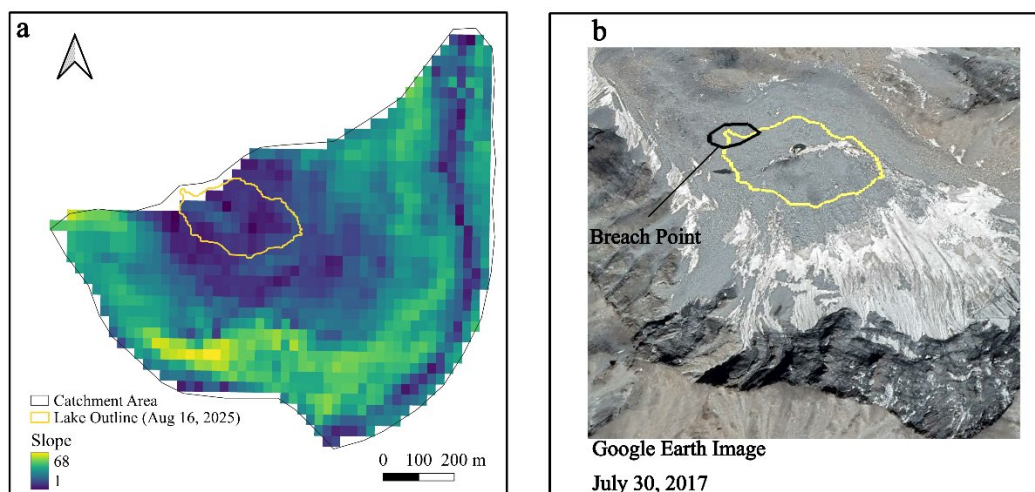


Figure 9. Terrain context of the breached glacial lake and surrounding catchment. (a) Slope derived from the SRTM DEM, with the pre-GLOF lake outline overlain highlights the steep and topographically complex terrain surrounding the lake. (b) Google Earth image of the same area shows the lake position relative to adjacent high-slope regions and near-vertical cliff walls in the upper catchment.

The optical evidence suggests that the 2025 GLOF was driven by meltwater inflow from seasonal snow leading to overtopping or erosion and dam failure rather than by a large landslide trigger. GPM IMERG daily precipitation time series shows several short-duration precipitation events during August 2025 (Figure S5), suggesting moist soils as well as runoff inputs to the lake. Fresh snowfall on August 20, as shown by PlanetScope imagery, at higher elevations within the steep, rapidly draining catchment and its disappearance by August 22 (Figure S4) implies meltwater input prior to the outburst. Although ERA5-Land temperature time series indicates above-freezing air temperatures during this period (Figure S5), the coarse spatial resolution (~9 km) of the reanalysis product may overestimate temperatures at the high elevations. The rapid melt of the fresh snowfall likely produced short-term inflow pulses to the lake, increasing hydrostatic pressure on the moraine dam and enhancing overtopping or erosional failure potential prior to the outburst.

Post-event imagery shows near-complete drainage of the lake, accompanied by widespread exposure of lakebed sediments and dam breach at the lowest point along the lake margin (Figure 10b). A narrow, elongate corridor of light-toned disturbed material extends downstream from the breach, following a pre-existing topographic low.

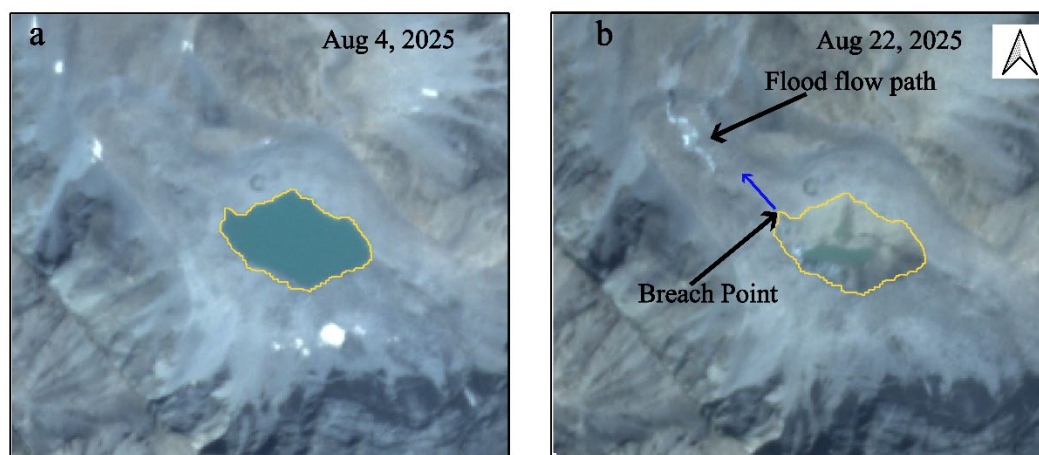


Figure 10. Pre- and post-event PlanetScope imagery of the glacial lake showing morphological changes associated with the 2025 GLOF. (a) The pre-event image shows the intact lake with the pre-GLOF lake outline

indicated. (b) The post-event image shows drained lake, breach point at the lowest lake margin, and a channelized flood-eroded and reworked sediment corridor extending downstream from the breach.

4. Discussion

4.1. Climatic and Cryospheric Controls on the 2025 GLOF

Among the wide range of documented GLOF trigger mechanisms, dynamic mass movements into lakes, such as landslides, avalanches, rockfalls, or glacier calving, are widely recognized as the dominant trigger type [7,24,53]. Such mass movements can rapidly displace lake water and generate high-energy displacement waves that overtop and erode moraine dams [10,14]. Hydrometeorological extremes, including intense rainfall or rapid ice and snowmelt during exceptionally high temperatures, can destabilize dams by abruptly raising lake levels and increasing hydrostatic pressure on dam structures [59–61]. In addition to these dynamic triggers, more gradual processes may lead to GLOFs, including continuous lake level rise resulting in overtopping or hydrostatic failure, as well as internal degradation mechanisms such as seepage, piping, and the thawing of ice-cored or permafrost-rich moraine materials that weaken dam stability over time [10,20,61,62].

The 2025 Talidas GLOF was most likely driven by a combination of anomalous climatic and cryospheric conditions rather than a discrete external trigger. Summer 2025 represented an extreme climatic outlier relative to the 2000-2024 baseline, characterized by a sustained positive thermal departure throughout the melt season. These persistently warm conditions likely enhanced catchment-wide snowmelt, accelerated lake growth, and resulted in unusually prolonged snow-free periods. The sustained rise in lake level would have progressively increased hydrostatic pressure on the moraine dam, promoting overtopping or erosional incision even in the absence of a sudden impact trigger.

In addition to meltwater input, permafrost conditions within the high-elevation catchment may have further contributed to dam destabilization. The high probability of permafrost suggests the presence of frozen ground and potentially ice-rich moraine materials within the lake basin and surrounding terrain. Prolonged snow-free conditions, combined with anomalously warm conditions across much of the summer, would have increased surface energy absorption, promoting ground warming and potential permafrost degradation [13,63]. Degradation of permafrost in steep alpine terrain can increase the likelihood of rockfalls and slope failure, while thawing of ice-rich moraine materials may reduce structural cohesion and enhance internal seepage and erosion [64]. Although no clear optical evidence of slope failure was observed in the catchment, progressive weakening of frozen or ice-rich dam materials and increased erosional susceptibility under sustained hydrostatic pressure remain plausible contributing factors.

Short-term hydrological pulses immediately prior to the outburst may have provided an additional destabilizing factor. The presence of fresh snow on August 20 on the upper slopes, followed by its disappearance by August 22, indicates a likely rapid melt event before the GLOF. In a steep, fast-draining catchment, rapid melt events can generate meltwater inflow over short timescales [64]. In addition, precipitation events during this period would have further increased catchment wetness and inflow to the lake. These short-lived melt and rainfall pulses, acting on an already stressed lake system, likely increased hydrostatic pressure on the moraine dam and contributed to overtopping or erosional breach.

In summary, the 2025 Talidas GLOF was most likely the result of compound climatic and cryospheric forcing. Lakes of comparable extent were observed in earlier years (e.g., 1994, 2004, and 2022) without documented outburst, indicating that maximum lake area alone did not control failure. In particular, during 2022-2024, the lake evolved more gradually, reached peak extent in mid-August, and subsequently contracted without abrupt drainage, while seasonal snow persisted throughout much of the summer, suggesting comparatively cooler melt-season conditions. In contrast, the 2025 lake exhibited rapid expansion, reached a similar maximum extent on a comparable seasonal timeline, and then underwent abrupt drainage. This divergence in behavior points to the importance

of environmental preconditioning in 2025 but also to the unpredictable nature of GLOF events. The concurrence of sustained warm temperatures, early and prolonged snow depletion, potential permafrost-related weakening of moraine materials, and short-term late-season inflows likely enhanced meltwater inflow and hydrostatic pressure while progressively reducing dam stability, ultimately leading to overtopping or erosional breach.

4.2. Implications for Remote Sensing-Based GLOF Monitoring and Early Warning

Remote sensing has emerged as an essential tool for the detection and monitoring of glacial lakes in remote, high-mountain regions where ground-based observations are limited or logistically impractical [65,66]. Multi-temporal satellite imagery enables systematic tracking of lake evolution, identification of changes in surrounding terrain, and assessment of potential GLOF hazards [67]. Advances in high-resolution optical and radar datasets have further improved the ability to reconstruct lake growth histories, evaluate geomorphic conditions, and quantify downstream impacts [68–70]. The increase in spatiotemporal resolution of satellite imagery and the number of available data sources (Figure 3) will improve monitoring and predicting GLOF risks. The integration of remotely sensed observations with climate and cryospheric data has also enhanced understanding of how meteorological forcing influences lake behavior and GLOF occurrence [14,25].

The Talidas GLOF event demonstrates the value of high-temporal-resolution satellite observations for capturing the complete life cycle of a hazardous glacial lake. The PlanetScope time series allowed detailed tracking of lake area changes at sub-weekly intervals, documenting the evolution of the lake through July and early August 2025, and the abrupt disappearance following catastrophic drainage. The results highlight the importance of monitoring not only lake areas but also their rate of change and surrounding geomorphic conditions, meteorological variability, and seasonal snow dynamics, all of which provided important context for understanding the rapid lake expansion and drainage.

These findings suggest that remote-sensing-based GLOF monitoring frameworks should move beyond a sole focus on maximum lake size. Greater emphasis should be placed on tracking the trajectory of lake growth, evaluating dam and catchment characteristics, and identifying potential triggering processes such as landslides, avalanches, glacier calving, anomalous meteorological conditions or gradual dam degradation. Historical lake behavior, as documented through multi-decadal satellite records, can provide critical context for assessing which lakes are exhibiting anomalous or hazardous development patterns, such as rapid lake growth. Incorporating indicators such as early snow cover depletion in lake catchments, anomalously warm temperatures, rapid or sustained increases in lake area, and observable geomorphological changes into routine monitoring protocols can improve the ability of remote sensing to support early-warning systems and proactive risk management. This study illustrates how dense time-series observations, when combined with climatic and cryospheric information, offer a practical and scalable foundation for GLOF surveillance in data-scarce mountain environments.

4.3. Limitations and Future Directions

Although this study benefited from high spatial resolution (3 m) PlanetScope imagery for mapping lake outlines, several sources of uncertainty remain. Manual delineation using high-resolution imagery reduces area estimation errors relative to coarser-resolution sensors, but shoreline mapping can still be affected by snow cover, cast shadows, turbid water, and variable illumination conditions [71–73]. Our analysis relied primarily on optical imagery, which is inherently constrained by cloud cover and seasonal weather conditions [66]. Nevertheless, the daily temporal resolution of PlanetScope imagery provided a sufficiently dense record to capture lake evolution and seasonal snow dynamics with minimal temporal gaps.

While pre- and post-event imagery allowed us to rule out external mass movement as a likely trigger of the 2025 GLOF, optical data alone are insufficient to fully diagnose failure mechanisms such as internal piping, ice-core degradation, or progressive dam weakening. The absence of in-situ

observations limits direct validation of remote-sensing-based interpretations and prevents detailed characterization of the dam structure and channel erosion processes. In addition, our interpretation of melt-season climatology relies on ERA5-Land reanalysis data (~9 km resolution), which may not fully resolve strong elevational gradients and microclimatic variability within small catchments. Previous studies have shown that ERA5 temperatures can overestimate observed values during pre-monsoon and monsoon periods in complex mountain terrain, reflecting limitations in representing fine-scale temperature fluctuations [74–76].

Future work could address these limitations through the integration of complementary datasets and methods. Synthetic Aperture Radar (SAR) imagery offers an all-weather alternative to optical observations and could enable more consistent monitoring of lake extent and surrounding slope conditions, particularly during periods of persistent cloud cover. Multi-temporal DEMs derived from stereo optical imagery or radar interferometry would allow estimation of volumetric changes in the lake basin and adjacent terrain, improving understanding of pre-failure lake dynamics and geomorphic precursors. Targeted field investigations, where feasible, would further strengthen interpretations by providing direct information on dam composition, subsurface conditions, and potential GLOF triggers.

Further, reconstruction of the 2025 GLOF, including post-breach flood routing, sediment transport analysis, and channel evolution mapping, would enhance understanding of downstream impacts and process dynamics. Combining optical time series, SAR observations, DEM analysis, and hydrodynamic modeling represent a promising pathway for improving the physical interpretation of GLOF processes and advancing remote-sensing-based early-warning frameworks in high-mountain regions.

5. Conclusion

This study documented the seasonal evolution and abrupt drainage of a moraine-dammed glacial lake in the Talidas catchment using a multi-sensor remote sensing framework. High-resolution PlanetScope imagery captured the full life cycle of the lake during the 2025 melt season, revealing initial lake formation in mid-June, sustained expansion through July and early August, and near-complete drainage on August 22, 2025. The lake reached a maximum area of 0.052 km² prior to the outburst, expanding by more than a factor of four over two months. Multi-decadal analysis using Landsat (1992-2018) and PlanetScope (2017-2024) imagery shows that lake formation in this catchment has historically been intermittent and short-lived, with no clear evidence of abrupt drainage events prior to 2025, highlighting the anomalous nature of the 2025 GLOF.

Integrated analysis of lake dynamics, seasonal snow cover, and temperature indicates that the 2025 event was most consistent with compound climatic and cryospheric forcing rather than a discrete external trigger. Summer 2025 was characterized by persistently warmer conditions relative to the 2000-2024 baseline, rapid seasonal snowmelt within the catchment, and early and prolonged snow-free conditions. These factors likely enhanced meltwater inflow and increased hydrostatic pressure on the moraine dam. The absence of identifiable landslide scars or impact deposits signals in pre- and post-event imagery further supports an overtopping or erosion-dominated failure mechanism driven by continuous lake growth and hydrostatic pressure rather than sudden displacement waves. The possible presence of permafrost within the catchment suggests an additional preconditioning mechanism, whereby sustained warm conditions may have weakened ice-rich moraine materials and reduced dam stability over the melt season. Short-term hydrological pulses associated with precipitation shortly before the outburst may have provided an additional hydrological input to an already critically filled lake.

This study demonstrates the critical value of high-temporal-resolution satellite observations for reconstructing hazardous glacial lake evolution in remote, data-scarce mountain regions. The integration of optical imagery (PlanetScope and Landsat), MODIS-based snow cover data, ERA5-Land temperature reanalysis, and permafrost probability datasets provided a comprehensive, multi-dimensional framework for diagnosing potential GLOF controls without field observations. This

highlights the growing role of multi-sensor remote sensing as a practical and scalable tool for GLOF monitoring and post-event forensic analysis in inaccessible alpine terrain. The results also have direct implications for remote-sensing-based GLOF monitoring and early-warning efforts. The Talidas case shows that indicators such as extreme temperatures, rapid and persistent snow depletion, lake expansion, and geomorphic observation of lake surroundings may collectively signal elevated outburst risk. Incorporating time-series analysis of snow dynamics, climatic anomalies, and lake growth trajectories can substantially improve the identification of anomalous and potentially hazardous lake evolution.

Supplementary Materials: The following supporting information can be downloaded at the website of this paper posted on Preprints.org. Figure S1: False color composite of PlanetScope image from August 04, 2025, showing multiple lakes upstream of the Talidas settlement. The lake at the highest elevation drained out on August 22, 2025, while the lakes below overflowed due to the flood wave but remained structurally intact and did not undergo catastrophic drainage; Table S1: Summary of remote sensing and reanalysis datasets used in this study, including sensor/source, temporal coverage, spatial resolution, and specific applications in the study; Table S2: Performance metrics for independent temporal validation of the Random Forest snow classification using manually digitized validation polygons from June 20, July 2, and July 21, 2025; Figure S2: Number of snow-free days in the lake catchment during the June-September period for 2000-2025 derived from MODIS observations. The horizontal blue line indicates the mean number of snow-free days for the 2000-2024 baseline. The chart shows that 2025 experienced the highest number of snow-free days in the 26-year record, reflecting exceptionally early and sustained seasonal snow depletion; Figure S3: Seasonal evolution of fSCA within the lake catchment for the 2022-2025 melt seasons. All years show rapid snow depletion during early summer followed by low and stable values in July-August. The 2025 season exhibits consistently lower fSCA and earlier transition to near-snow-free conditions compared to the preceding years; Figure S4: False color composite of PlanetScope image from August 20, 2025, showing fresh snow on the higher elevation slope upstream of the lake, which disappeared in addition to the drainage of the lake by the August 22, 2025, image; Figure S5: Daily areal-mean precipitation over the lake catchment during August 2025 derived from GPM IMERG V07 dataset and daily temperature derived from ERA5-Land dataset. The precipitation pulses preceding the outburst suggest additional short-term hydrometeorological inflow and moist soil.

Author Contributions: Conceptualization, I.K.; methodology, I.K. and J.M.J. (Jeremy M. Johnston); software, I.K.; validation, I.K.; formal analysis, I.K.; investigation, I.K.; resources, J.M.J. (Jennifer M. Jacobs); data curation, I.K.; writing—original draft preparation, I.K.; writing—review and editing, I.K., J.M.J. (Jeremy M. Johnston), and J.M.J. (Jennifer M. Jacobs); visualization, I.K.; supervision, J.M.J. (Jennifer M. Jacobs); project administration, J.M.J. (Jennifer M. Jacobs); funding acquisition, I.K. All authors have read and agreed to the published version of the manuscript.

Funding: This research was funded by a Fulbright Program grant sponsored by the Bureau of Educational and Cultural Affairs of the United States Department of State and administered by the Institute of International Education.

Data Availability Statement: The original contributions presented in this study are included in the article/Supplementary Material. Further inquiries can be directed to the corresponding author.

Conflicts of Interest: The authors declare no conflicts of interest. The funders had no role in the design of the study; in the collection, analyses, or interpretation of data; in the writing of the manuscript; or in the decision to publish the results.

Abbreviations

The following abbreviations are used in this manuscript:

ETM+	Enhanced Thematic Mapper Plus
fSCA	Fractional Snow-covered Area
GIS	Geographic Information System

GLOF	Glacial Lake Outburst Flood
GPM	Global Precipitation Measurement
IMERG	Integrated Multi-satellite Retrievals
MODIS	Moderate Resolution Imaging Spectroradiometer
NIR	Near Infrared
OLI	Operational Land Imager
RF	Random Forest
SAR	Synthetic Aperture Radar
SCA	Snow-covered Area
SD	Standard Deviation
SRTM	Shuttle Radar Topography Mission
TM	Thematic Mapper
USGS	United States Geological Survey

References

1. Clague, J. J.; Huggel, C.; Korup, O.; McGuire, B. Climate Change and Hazardous Processes in High Mountains. **2012**. <https://doi.org/10.5167/UZH-77920>.
2. Zhang, T.; Wang, W.; An, B. Heterogeneous Changes in Global Glacial Lakes under Coupled Climate Warming and Glacier Thinning. *Commun Earth Environ* **2024**, *5* (1), 374. <https://doi.org/10.1038/s43247-024-01544-y>.
3. Song, C.; Fan, C.; Ma, J.; Zhan, P.; Deng, X. A Spatially Constrained Remote Sensing-Based Inventory of Glacial Lakes Worldwide. *Sci Data* **2025**, *12* (1), 464. <https://doi.org/10.1038/s41597-025-04809-z>.
4. Shugar, D. H.; Burr, A.; Haritashya, U. K.; Kargel, J. S.; Watson, C. S.; Kennedy, M. C.; Bevington, A. R.; Betts, R. A.; Harrison, S.; Strattman, K. Rapid Worldwide Growth of Glacial Lakes since 1990. *Nat. Clim. Chang.* **2020**, *10* (10), 939–945. <https://doi.org/10.1038/s41558-020-0855-4>.
5. Zhang, T.; Wang, W.; An, B.; Wei, L. Enhanced Glacial Lake Activity Threatens Numerous Communities and Infrastructure in the Third Pole. *Nat Commun* **2023**, *14* (1), 8250. <https://doi.org/10.1038/s41467-023-44123-z>.
6. Ke, L.; Ding, X.; Ning, Y.; Liao, Y.; Song, C. Annual Trajectory of Global Glacial Lake Variations and the Interactions with Glacier Mass Balance during 2013–2022. *CATENA* **2024**, *245*, 108280. <https://doi.org/10.1016/j.catena.2024.108280>.
7. Richardson, S. D.; Reynolds, J. M. An Overview of Glacial Hazards in the Himalayas. *Quaternary International* **2000**, *65–66*, 31–47. [https://doi.org/10.1016/S1040-6182\(99\)00035-X](https://doi.org/10.1016/S1040-6182(99)00035-X).
8. Taylor, C.; Robinson, T. R.; Dunning, S.; Rachel Carr, J.; Westoby, M. Glacial Lake Outburst Floods Threaten Millions Globally. *Nat Commun* **2023**, *14* (1), 487. <https://doi.org/10.1038/s41467-023-36033-x>.
9. Emmer, A.; Allen, S. K.; Carey, M.; Frey, H.; Huggel, C.; Korup, O.; Mergili, M.; Sattar, A.; Veh, G.; Chen, T. Y.; Cook, S. J.; Correas-Gonzalez, M.; Das, S.; Diaz Moreno, A.; Drenkhan, F.; Fischer, M.; Immerzeel, W. W.; Izagirre, E.; Joshi, R. C.; Kougkoulos, I.; Kuyakanon Knapp, R.; Li, D.; Majeed, U.; Matti, S.; Moulton, H.; Nick, F.; Piroton, V.; Rashid, I.; Reza, M.; Ribeiro De Figueiredo, A.; Riveros, C.; Shrestha, F.; Shrestha, M.; Steiner, J.; Walker-Crawford, N.; Wood, J. L.; Yde, J. C. Progress and Challenges in Glacial Lake Outburst Flood Research (2017–2021): A Research Community Perspective. *Nat. Hazards Earth Syst. Sci.* **2022**, *22* (9), 3041–3061. <https://doi.org/10.5194/nhess-22-3041-2022>.
10. Emmer, A.; Cochachin, A. The Causes and Mechanisms of Moraine-Dammed Lake Failures in the Cordillera Blanca, North American Cordillera, and Himalayas. *AUC GEOGRAPHICA* **2013**, *48* (2), 5–15. <https://doi.org/10.14712/23361980.2014.23>.
11. Allen, S. K.; Rastner, P.; Arora, M.; Huggel, C.; Stoffel, M. Lake Outburst and Debris Flow Disaster at Kedarnath, June 2013: Hydrometeorological Triggering and Topographic Predisposition. *Landslides* **2015**, *13* (6), 1479–1491. <https://doi.org/10.1007/s10346-015-0584-3>.
12. Huggel, C.; Carey, M.; Emmer, A.; Frey, H.; Walker-Crawford, N.; Wallimann-Helmer, I. Anthropogenic Climate Change and Glacier Lake Outburst Flood Risk: Local and Global Drivers and Responsibilities for the Case of Lake Palcacocha, Peru. *Nat. Hazards Earth Syst. Sci.* **2020**, *20* (8), 2175–2193. <https://doi.org/10.5194/nhess-20-2175-2020>.

13. Yang, L.; Lu, Z.; Zhao, C.; Kim, J.; Yang, C.; Wang, B.; Liu, X.; Wang, Z. Analyzing the Triggering Factors of Glacial Lake Outburst Floods with SAR and Optical Images: A Case Study in Jinweng Co, Tibet, China. *Landslides* **2022**, *19* (4), 855–864. <https://doi.org/10.1007/s10346-021-01831-1>.
14. Yang, L.; Lu, Z.; Zhao, C.; Zhang, Q.; Hu, X.; Wang, B. Triggering Factors and Flooding Processes of Glacial Lake Outburst Flood at Ranzerio Lake. *npj Nat. Hazards* **2025**, *2* (1), 90. <https://doi.org/10.1038/s44304-025-00147-7>.
15. Thompson, S. S.; Kulesa, B.; Benn, D. I.; Mertes, J. R. Anatomy of Terminal Moraine Segments and Implied Lake Stability on Ngozumpa Glacier, Nepal, from Electrical Resistivity Tomography (ERT). *Sci Rep* **2017**, *7* (1), 46766. <https://doi.org/10.1038/srep46766>.
16. Sattar, A.; Goswami, A.; Kulkarni, A. V.; Emmer, A.; Haritashya, U. K.; Allen, S.; Frey, H.; Huggel, C. Future Glacial Lake Outburst Flood (GLOF) Hazard of the South Lhonak Lake, Sikkim Himalaya. *Geomorphology* **2021**, *388*. <https://doi.org/10.1016/j.geomorph.2021.107783>.
17. Mou, Y.; Chen, H.; Wang, T.; Ruan, H.; Li, X.; Yu, Y.; Zhou, Y.; Meng, H. The Breaching Mechanism of Moraine Dams with Buried Ice: A Review. *Cold Regions Science and Technology* **2024**, *228*, 104315. <https://doi.org/10.1016/j.coldregions.2024.104315>.
18. Yao, T.; Thompson, L.; Yang, W.; Yu, W.; Gao, Y.; Guo, X.; Yang, X.; Duan, K.; Zhao, H.; Xu, B.; Pu, J.; Lu, A.; Xiang, Y.; Kattel, D. B.; Joswiak, D. Different Glacier Status with Atmospheric Circulations in Tibetan Plateau and Surroundings. *Nature Clim Change* **2012**, *2* (9), 663–667. <https://doi.org/10.1038/nclimate1580>.
19. Nie, Y.; Sheng, Y.; Liu, Q.; Liu, L.; Liu, S.; Zhang, Y.; Song, C. A Regional-Scale Assessment of Himalayan Glacial Lake Changes Using Satellite Observations from 1990 to 2015. *Remote Sensing of Environment* **2017**, *189*, 1–13. <https://doi.org/10.1016/j.rse.2016.11.008>.
20. Harrison, S.; Kargel, J. S.; Huggel, C.; Reynolds, J.; Shugar, D. H.; Betts, R. A.; Emmer, A.; Glasser, N.; Haritashya, U. K.; Klimeš, J.; Reinhardt, L.; Schaub, Y.; Wiltshire, A.; Regmi, D.; Vilimek, V. Climate Change and the Global Pattern of Moraine-Dammed Glacial Lake Outburst Floods. *The Cryosphere* **2018**, *12* (4), 1195–1209. <https://doi.org/10.5194/tc-12-1195-2018>.
21. Chen, N.; Liu, M.; Allen, S.; Deng, M.; Khanal, N. R.; Peng, T.; Tian, S.; Huggel, C.; Wu, K.; Rahman, M.; Somos-Valenzuela, M. Small Outbursts into Big Disasters: Earthquakes Exacerbate Climate-Driven Cascade Processes of the Glacial Lakes Failure in the Himalayas. *Geomorphology* **2023**, *422*, 108539. <https://doi.org/10.1016/j.geomorph.2022.108539>.
22. Rinzin, S.; Zhang, G.; Sattar, A.; Wangchuk, S.; Allen, S. K.; Dunning, S.; Peng, M. GLOF Hazard, Exposure, Vulnerability, and Risk Assessment of Potentially Dangerous Glacial Lakes in the Bhutan Himalaya. *Journal of Hydrology* **2023**, *619*, 129311. <https://doi.org/10.1016/j.jhydrol.2023.129311>.
23. Emmer, A.; Vilca, O.; Salazar Checa, C.; Li, S.; Cook, S.; Pummer, E.; Hrebrina, J.; Haeberli, W. Causes, Consequences and Implications of the 2023 Landslide-Induced Lake Rasac Glacial Lake Outburst Flood (GLOF), Cordillera Huayhuash, Peru. *Nat. Hazards Earth Syst. Sci.* **2025**, *25* (3), 1207–1228. <https://doi.org/10.5194/nhess-25-1207-2025>.
24. Zhang, T.; Wang, W.; Kougkoulos, I.; Cook, S. J.; Li, S.; Iribarren-Anacona, P.; Watson, C. S.; An, B.; Yao, T. High Frequency of Moraine-Dammed Lake Outburst Floods Driven by Global Warming. *Nat Commun* **2025**, *16* (1), 11173. <https://doi.org/10.1038/s41467-025-67650-3>.
25. Sattar, A.; Haritashya, U. K.; Kargel, J. S.; Karki, A. Transition of a Small Himalayan Glacier Lake Outburst Flood to a Giant Transborder Flood and Debris Flow. *Sci Rep* **2022**, *12* (1), 12421. <https://doi.org/10.1038/s41598-022-16337-6>.
26. Neupane, R.; Chen, H.; Cao, C. Review of Moraine Dam Failure Mechanism. *Geomatics, Natural Hazards and Risk* **2019**, *10* (1), 1948–1966. <https://doi.org/10.1080/19475705.2019.1652210>.
27. Veh, G.; Lützow, N.; Tamm, J.; Luna, L. V.; Hugonnet, R.; Vogel, K.; Geertsema, M.; Clague, J. J.; Korup, O. Less Extreme and Earlier Outbursts of Ice-Dammed Lakes since 1900. *Nature* **2023**, *614* (7949), 701–707. <https://doi.org/10.1038/s41586-022-05642-9>.
28. Ahmed, R. Decoding the Fate of Himalayan Glaciers under Climate Change: Impacts, Challenges, Research Gaps, and Policy Pathways. *Evolving Earth* **2025**, *3*, 100082. <https://doi.org/10.1016/j.eve.2025.100082>.
29. Sattar, A.; Cook, K. L.; Rai, S. K.; Berthier, E.; Allen, S.; Rinzin, S.; De Vries, M. V. W.; Haeberli, W.; Kushwaha, P.; Shugar, D. H.; Emmer, A.; Haritashya, U. K.; Frey, H.; Rao, P.; Gurudin, K. S. K.; Rai, P.;

- Rajak, R.; Hossain, F.; Huggel, C.; Mergili, M.; Azam, Mohd. F.; Gascoin, S.; Carrivick, J. L.; Bell, L. E.; Ranjan, R. K.; Rashid, I.; Kulkarni, Anil. V.; Petley, D.; Schwanghart, W.; Watson, C. S.; Islam, N.; Gupta, M. D.; Lane, S. N.; Bhat, S. Y. The Sikkim Flood of October 2023: Drivers, Causes, and Impacts of a Multihazard Cascade. *Science* **2025**, *387* (6740), eads2659. <https://doi.org/10.1126/science.ads2659>.
30. Westoby, M. J.; Glasser, N. F.; Brasington, J.; Hambrey, M. J.; Quincey, D. J.; Reynolds, J. M. Modelling Outburst Floods from Moraine-Dammed Glacial Lakes. *Earth-Science Reviews* **2014**, *134*, 137–159. <https://doi.org/10.1016/j.earscirev.2014.03.009>.
 31. Carrivick, J. L.; Tweed, F. S. A Global Assessment of the Societal Impacts of Glacier Outburst Floods. *Global and Planetary Change* **2016**, *144*, 1–16. <https://doi.org/10.1016/j.gloplacha.2016.07.001>.
 32. Peng, M.; Wang, X.; Zhang, G.; Veh, G.; Sattar, A.; Chen, W.; Allen, S. Cascading Hazards from Two Recent Glacial Lake Outburst Floods in the Nyainqêntanglha Range, Tibetan Plateau. *Journal of Hydrology* **2023**, *626*, 130155. <https://doi.org/10.1016/j.jhydrol.2023.130155>.
 33. Zhang, G.; Carrivick, J. L.; Emmer, A.; Shugar, D. H.; Veh, G.; Wang, X.; Labeledz, C.; Mergili, M.; Mölg, N.; Huss, M.; Allen, S.; Sugiyama, S.; Lützwow, N. Characteristics and Changes of Glacial Lakes and Outburst Floods. *Nat Rev Earth Environ* **2024**, *5* (6), 447–462. <https://doi.org/10.1038/s43017-024-00554-w>.
 34. Wilson, R.; Harrison, S.; Reynolds, J.; Hubbard, A.; Glasser, N. F.; Wünderlich, O.; Iribarren Anaconda, P.; Mao, L.; Shannon, S. The 2015 Chileno Valley Glacial Lake Outburst Flood, Patagonia. *Geomorphology* **2019**, *332*, 51–65. <https://doi.org/10.1016/j.geomorph.2019.01.015>.
 35. Izagirre, E.; Casassa, G.; Dussailant, I.; Miles, E. S.; Wilson, R.; Rada, C.; Faria, S. H.; Antigüedad, I. Evolution of Glacial Lakes and Southernmost GLOFs in the Cordillera Darwin and Cloue Icefields (Tierra Del Fuego) between 1945–2024. *Front. Earth Sci.* **2025**, *13*, 1641167. <https://doi.org/10.3389/feart.2025.1641167>.
 36. Ahmed, R. Glacial Lake Outburst Flood (GLOF) Hazard and Risk Management Strategies: A Global Overview. *Water Resour Manage* **2025**, *39* (1), 1–16. <https://doi.org/10.1007/s11269-024-03958-x>.
 37. Tom, M.; Odermatt, D.; David, C. H.; Cerbelaud, A.; Wade, J.; Frey, H. Monitoring Earth's Glacial Lakes from Space with Machine Learning. *Science of Remote Sensing* **2025**, *12*, 100277. <https://doi.org/10.1016/j.srs.2025.100277>.
 38. DAWN. 200 People Rescued after Glacial Burst in Gilgit-Baltistan's Ghizer: Rescue 1122. Pakistan August 22, 2025. <https://www.dawn.com/news/1933779> (accessed 2026-02-20).
 39. RGI Consortium. Randolph Glacier Inventory - A Dataset of Global Glacier Outlines, Version 7, 2023. <https://doi.org/10.5067/F6JMOVY5NAVZ>.
 40. Hussain, N.; Ali, S.; Hussain, A.; Ali, S.; Khan, S.; Raza, G.; Abbas, Q.; Hussain, I.; Hussain, M. Climate Change Variability Trends and Implications for Freshwater Resources in Pakistan's Eastern Hindu Kush Region. *Pol. J. Environ. Stud.* **2018**, *27* (2), 665–673. <https://doi.org/10.15244/pjoes/75960>.
 41. Adnan, M.; Nabi, G.; Kang, S.; Zhang, G.; Adnan, R. M.; Anjum, M. N.; Iqbal, M.; Ali, A. F. Snowmelt Runoff Modelling under Projected Climate Change Patterns in the Gilgit River Basin of Northern Pakistan. *Pol. J. Environ. Stud.* **2017**, *26* (2), 525–542. <https://doi.org/10.15244/pjoes/66719>.
 42. Hewitt, K. Glacier Change, Concentration, and Elevation Effects in the Karakoram Himalaya, Upper Indus Basin. *Mountain Research and Development* **2011**, *31* (3), 188–200. <https://doi.org/10.1659/mrd-journal-d-11-00020.1>.
 43. Hasson, S.; Lucarini, V.; Khan, M. R.; Petitta, M.; Bolch, T.; Gioli, G. Early 21st Century Snow Cover State over the Western River Basins of the Indus River System. *Hydrol. Earth Syst. Sci.* **2014**, *18* (10), 4077–4100. <https://doi.org/10.5194/hess-18-4077-2014>.
 44. Adnan, M.; Liu, S.; Saifullah, M.; Iqbal, M.; Saddique, Q.; Ul Hussan, W.; Latif, Y. Estimation of Changes in Runoff and Its Sources in Response to Future Climate Change in a Critical Zone of the Karakoram Mountainous Region, Pakistan in the near and Far Future. *Geomatics, Natural Hazards and Risk* **2024**, *15* (1), 2291330. <https://doi.org/10.1080/19475705.2023.2291330>.
 45. John, A.; Cannistra, A. F.; Yang, K.; Tan, A.; Shean, D.; Hille Ris Lambers, J.; Cristea, N. High-Resolution Snow-Covered Area Mapping in Forested Mountain Ecosystems Using PlanetScope Imagery. *Remote Sensing* **2022**, *14* (14), 3409. <https://doi.org/10.3390/rs14143409>.

46. Wang, Z.; Jaya Baskar, J. V.; Sistla Naga Sai, M. S.; Svoma, B.; Vivoni, E. R. Spatiotemporal Patterns of Intermittent Snow Cover From PlanetScope Imagery Using Deep Learning. *Geophysical Research Letters* **2025**, *52* (13), e2025GL116582. <https://doi.org/10.1029/2025GL116582>.
47. Frazier, A. E.; Hemingway, B. L. A Technical Review of Planet Smallsat Data: Practical Considerations for Processing and Using PlanetScope Imagery. *Remote Sensing* **2021**, *13* (19), 3930. <https://doi.org/10.3390/rs13193930>.
48. Shields, S. G.; Coops, N. C.; Achim, A.; Hamelin, R. C.; Mulverhill, C. A Review of PlanetScope CubeSats for Forest Monitoring. *Science of Remote Sensing* **2025**, *12*, 100314. <https://doi.org/10.1016/j.srs.2025.100314>.
49. Yang, K.; John, A.; Shean, D.; Lundquist, J. D.; Sun, Z.; Yao, F.; Todoran, S.; Cristea, N. High-Resolution Mapping of Snow Cover in Montane Meadows and Forests Using Planet Imagery and Machine Learning. *Front. Water* **2023**, *5*, 1128758. <https://doi.org/10.3389/frwa.2023.1128758>.
50. Johnston, J.; Jacobs, J.; Cho, E. MODIS/Terra Global Annual 0.01Deg CMG Snow Cover Climatology, Version 1, 2024. <https://doi.org/10.5067/9R1AM6NNZLTV>.
51. Farr, T. G.; Rosen, P. A.; Caro, E.; Crippen, R.; Duren, R.; Hensley, S.; Kobrick, M.; Paller, M.; Rodriguez, E.; Roth, L.; Seal, D.; Shaffer, S.; Shimada, J.; Umland, J.; Werner, M.; Oskin, M.; Burbank, D.; Alsdorf, D. The Shuttle Radar Topography Mission. *Reviews of Geophysics* **2007**, *45* (2), 2005RG000183. <https://doi.org/10.1029/2005RG000183>.
52. Hersbach, H.; Bell, B.; Berrisford, P.; Hirahara, S.; Horányi, A.; Muñoz-Sabater, J.; Nicolas, J.; Peubey, C.; Radu, R.; Schepers, D.; Simmons, A.; Soci, C.; Abdalla, S.; Abellan, X.; Balsamo, G.; Bechtold, P.; Biavati, G.; Bidlot, J.; Bonavita, M.; De Chiara, G.; Dahlgren, P.; Dee, D.; Diamantakis, M.; Dragani, R.; Flemming, J.; Forbes, R.; Fuentes, M.; Geer, A.; Haimberger, L.; Healy, S.; Hogan, R. J.; Hólm, E.; Janisková, M.; Keeley, S.; Laloyaux, P.; Lopez, P.; Lupu, C.; Radnoti, G.; De Rosnay, P.; Rozum, I.; Vamborg, F.; Villaume, S.; Thépaut, J. The ERA5 Global Reanalysis. *Quart J Royal Meteor Soc* **2020**, *146* (730), 1999–2049. <https://doi.org/10.1002/qj.3803>.
53. Huffman, G.; Bolvin, D.; Braithwaite, D.; Hsu, K.; Joyce, R.; Xie, P. Integrated Multi-satellitE Retrievals for GPM (IMERG), 2014.
54. Kim, K. Y.; Lakshmi, V.; Rajaram, H.; Kansara, P.; Haagenson, R. High Mountain Asia 1 Km MODIS-AIRS Gap-Filled Ground Temperatures and Permafrost Probability Maps, 2003-2016, Version 1, 2024. <https://doi.org/10.5067/ZSRHP8H3GGSK>.
55. Hu, J. M.; Shean, D. Improving Mountain Snow and Land Cover Mapping Using Very-High-Resolution (VHR) Optical Satellite Images and Random Forest Machine Learning Models. *Remote Sensing* **2022**, *14* (17), 4227. <https://doi.org/10.3390/rs14174227>.
56. Johnston, J. M.; Jacobs, J. M.; Hunsaker, A.; Wagner, C.; Vardaman, M. Applications of Snow-Covered Areas from Unoccupied Aerial Systems (UAS) Visible Imagery: A Demonstration in Southeastern New Hampshire. *Remote Sensing* **2025**, *17* (11), 1885. <https://doi.org/10.3390/rs17111885>.
57. Moradi, M.; Fleming, A. G.; Hunsaker, A.; Jacobs, J. M. Identifying Snow-Covered Areas from Unoccupied Aerial Systems (UAS) Visible Imagery: A Comparison of Methods. *Snow/Remote Sensing* October 1, 2025. <https://doi.org/10.5194/egusphere-2025-4371>.
58. Furian, W.; Loibl, D.; Schneider, C. Future Glacial Lakes in High Mountain Asia: An Inventory and Assessment of Hazard Potential from Surrounding Slopes. *J. Glaciol.* **2021**, *67* (264), 653–670. <https://doi.org/10.1017/jog.2021.18>.
59. Allen, S. K.; Rastner, P.; Arora, M.; Huggel, C.; Stoffel, M. Lake Outburst and Debris Flow Disaster at Kedarnath, June 2013: Hydrometeorological Triggering and Topographic Predisposition. *Landslides* **2016**, *13* (6), 1479–1491. <https://doi.org/10.1007/s10346-015-0584-3>.
60. Cook, K. L.; Andermann, C.; Gimbert, F.; Adhikari, B. R.; Hovius, N. Glacial Lake Outburst Floods as Drivers of Fluvial Erosion in the Himalaya. *Science* **2018**, *362* (6410), 53–57. <https://doi.org/10.1126/science.aat4981>.
61. Shrestha, F.; Steiner, J. F.; Shrestha, R.; Dhungel, Y.; Joshi, S. P.; Inglis, S.; Ashraf, A.; Wali, S.; Walizada, K. M.; Zhang, T. A Comprehensive and Version-Controlled Database of Glacial Lake Outburst Floods in High Mountain Asia. *Earth Syst. Sci. Data* **2023**, *15* (9), 3941–3961. <https://doi.org/10.5194/essd-15-3941-2023>.

62. Mool, P. K.; Joshi, S. P.; Bajracharya, S. R. *Inventory of Glaciers, Glacial Lakes and Glacial Lake Outburst Floods Monitoring and Early Warning Systems in the Hindu Kush - Himalayan Region, Nepal*; International Centre for Integrated Mountain Development: Kathmandu, 2001.
63. Oriana, L.-P.; Timo, S.; Nicola, D.; Tom, B. I. Towards a Better Understanding of River Network Dynamics in a Glacierized Catchment. *Journal of Hydrology* **2026**, *668*, 135029. <https://doi.org/10.1016/j.jhydrol.2026.135029>.
64. Allen, S.; Frey, H.; Huggel, C. *Assessment of Glacier and Permafrost Hazards in Mountain Regions. Technical Guidance Document*; Standing Group on Glacier and Permafrost Hazards in Mountains (GAPHAZ); International Association of Cryospheric Sciences (IACS) and the International Permafrost Association (IPA): Zurich, Switzerland / Lima, Peru, 2017; p 72. <https://www.researchgate.net/doi/10.13140/RG.2.2.26332.90245> (accessed 2026-02-12).
65. Kirschbaum, D.; Watson, C. S.; Rounce, D. R.; Shugar, D. H.; Kargel, J. S.; Haritashya, U. K.; Amatya, P.; Shean, D.; Anderson, E. R.; Jo, M. The State of Remote Sensing Capabilities of Cascading Hazards Over High Mountain Asia. *Front. Earth Sci.* **2019**, *7*, 197. <https://doi.org/10.3389/feart.2019.00197>.
66. Khan, I.; Vardaman, M.; Johnston, J.; Jacobs, J. M. Glacial Lake Mapping: Progress, Challenges, and Future Directions. *Arctic, Antarctic, and Alpine Research* **2025**, *57* (1), 2592365. <https://doi.org/10.1080/15230430.2025.2592365>.
67. Nurakynov, S.; Sydyk, N.; Baygurin, Z.; Balakay, L. Advancements in Remote Sensing for Monitoring and Risk Assessment of Glacial Lake Outburst Floods. *Geosciences* **2025**, *15* (6), 211. <https://doi.org/10.3390/geosciences15060211>.
68. Khanal, N. R.; Mool, P. K.; Shrestha, A. B.; Rasul, G.; Ghimire, P. K.; Shrestha, R. B.; Joshi, S. P. A Comprehensive Approach and Methods for Glacial Lake Outburst Flood Risk Assessment, with Examples from Nepal and the Transboundary Area. *International Journal of Water Resources Development* **2015**, *31* (2), 219–237. <https://doi.org/10.1080/07900627.2014.994116>.
69. Sattar, A.; Goswami, A.; Kulkarni, Anil. V.; Emmer, A.; Haritashya, U. K.; Allen, S.; Frey, H.; Huggel, C. Future Glacial Lake Outburst Flood (GLOF) Hazard of the South Lhonak Lake, Sikkim Himalaya. *Geomorphology* **2021**, *388*, 107783. <https://doi.org/10.1016/j.geomorph.2021.107783>.
70. Yang, L.; Lu, Z.; Ouyang, C.; Zhao, C.; Hu, X.; Zhang, Q. Glacial Lake Outburst Flood Monitoring and Modeling through Integrating Multiple Remote Sensing Methods and HEC-RAS. *Remote Sensing* **2023**, *15* (22), 5327. <https://doi.org/10.3390/rs15225327>.
71. Li, J.; Warner, T. A.; Wang, Y.; Bai, J.; Bao, A. Mapping Glacial Lakes Partially Obscured by Mountain Shadows for Time Series and Regional Mapping Applications. *International Journal of Remote Sensing* **2019**, *40* (2), 615–641. <https://doi.org/10.1080/01431161.2018.1516314>.
72. Wangchuk, S.; Bolch, T. Mapping of Glacial Lakes Using Sentinel-1 and Sentinel-2 Data and a Random Forest Classifier: Strengths and Challenges. *Science of Remote Sensing* **2020**, *2*, 100008. <https://doi.org/10.1016/j.srs.2020.100008>.
73. Bazilova, V.; Käab, A. Mapping Area Changes of Glacial Lakes Using Stacks of Optical Satellite Images. *Remote Sensing* **2022**, *14* (23), 5973. <https://doi.org/10.3390/rs14235973>.
74. Xu, W.; Lei, X.; Chen, S.; Yu, T.; Hu, Z.; Zhang, M.; Jiang, L.; Bao, R.; Guan, X.; Ma, M.; Wei, J.; Gao, L.; Feng, A. How Well Does the ERA5 Reanalysis Capture the Extreme Climate Events Over China? Part II: Extreme Temperature. *Front. Environ. Sci.* **2022**, *10*, 921659. <https://doi.org/10.3389/fenvs.2022.921659>.
75. Lopes, F. M.; Dutra, E.; Boussetta, S. Evaluation of Daily Temperature Extremes in the ECMWF Operational Weather Forecasts and ERA5 Reanalysis. *Atmosphere* **2024**, *15* (1), 93. <https://doi.org/10.3390/atmos15010093>.
76. Satyapragyan, S.; Yadav, J. S.; Bhambri, R. Bias Corrections of ERA5 and ERA5-Land Temperature Using Automatic Weather Station Data in the Higher Central Himalaya: Implications for Hydro-Meteorological and Glaciological Research. *Journal of Hydrology: Regional Studies* **2026**, *63*, 103079. <https://doi.org/10.1016/j.ejrh.2025.103079>.

Disclaimer/Publisher's Note: The statements, opinions and data contained in all publications are solely those of the individual author(s) and contributor(s) and not of MDPI and/or the editor(s). MDPI and/or the editor(s) disclaim responsibility for any injury to people or property resulting from any ideas, methods, instructions or products referred to in the content.